Scilight

Bioresource Circularity & Carbon Neutrality

https://www.sciltp.com/journals/bccn



Article

Comparative GC-MS Metabolite Profiling and Physicochemical Characterization of *Eichhornia crassipes* Biomass Fractions across Diverse Aquatic Habitats

Sagar Aditya [1,*] and Ajay S. Kalamdhad [1,2]

[1] School of Agro and Rural Technology, Indian Institute of Technology Guwahati, Assam 781039, India
[2] Department of Civil Engineering, Indian Institute of Technology Guwahati, Assam 781039, India
* Correspondence: sagar.aditya@iitg.ac.in

How To Cite: Aditya, S.; Kalamdhad, A.S. Comparative GC-MS Metabolite Profiling and Physicochemical Characterization of *Eichhornia crassipes* Biomass Fractions across Diverse Aquatic Habitats. *Bioresource Circularity & Carbon Neutrality* **2026**, *1*(1), 2.

Received: 30 June 2026
Revised: 4 August 2026
Accepted: 27 August 2026
Published: 18 September 2026

Abstract: The rapid spread of the aquatic macrophyte water hyacinth (*Eichhornia crassipes*) has become a major ecological concern. This study evaluated the physicochemical, structural, and chemical characteristics of water hyacinth biomass collected from four different environments (freshwater bodies, near Boragaon dump sites, agricultural run-off areas, and industrial areas). The physicochemical properties varied across the sampling locations and plant parts. Samples collected from the Boragaon area showed the total nitrogen content ranged from 1.99% to 3.68%. Organic matter content ranged from 81.04% to 81.39% in leaf and stem samples from the industrial area, whereas root and whole-plant samples from Boragaon showed values ranging from 76.69% to 84.30%. The highest total phosphorus content (3585 mg/kg) was recorded in stem samples from Boragaon, while the lowest value (315 mg/kg) was found in root samples from the freshwater body. Heavy metal analysis also showed differences among the sampling locations, with the highest Cd concentration (1.09 mg/kg) recorded in whole-plant samples collected from the industrial area. These variations indicate that the surrounding environmental conditions and degree of pollution may influence the composition and potential utilization of *E. crassipes* biomass. Fourier Transform infrared (FTIR) analysis showed variations in polysaccharide-related bands, aromatic structures, and oxygen-containing functional groups in the different samples. Gas Chromatography-Mass Spectrometry (GC-MS) analysis further identified a broad spectrum of fatty acid derivatives, phenolic compounds, hydrocarbons, and organic acids, with their occurrence varying across sampling locations. These findings provide a location-specific basis for assessing the suitability of water hyacinth biomass for various industrial bioresource uses and stress the importance of accounting for environmental conditions during biomass evaluation.

Keywords: *Eichhornia crassipes*; physicochemical characterization; environmental pollution; FTIR; GC-MS metabolites

1. Introduction

Water hyacinth (*Eichhornia crassipes*), a non-native, free-floating invasive macrophyte, is recognized globally as one of the most aggressive aquatic weeds due to its extraordinary proliferation rate and dense mat formation. Its rapid spread in freshwater systems obstructs navigation, irrigation infrastructure, fisheries, and hydropower generation, creating serious ecological and socio-economic challenges [1,2].

It shows high biomass productivity and a strong ability to remove pollutants from contaminated water. Morphologically, mature plants are characterized by fibrous pendant roots, rhizomes, stolons, glossy leaves, and

Copyright: © 2026 by the authors. This is an open access article under the terms and conditions of the Creative Commons Attribution (CC BY) license (https://creativecommons.org/licenses/by/4.0/).
Publisher's Note: Scilight stays neutral with regard to jurisdictional claims in published maps and institutional affiliations.

bearing 6–10 lilac to violet flowers, each 4–7 cm in diameter. While individual plants can reach up to 1 m, an average height of around 40 cm is more common. The presence of aerenchymatous tissues within petioles and stems provides buoyancy, enabling free-floating growth. Reproduction occurs primarily through sexual reproduction via seeds, which is also possible [3,4]. Water hyacinth is considered one of the most productive plant species globally, with annual dry biomass productivity of approximately 50 kg/m^2 [4,5]. Dense mats can host up to two million plants per hectare, with total biomass ranging from 270 to 400 tons [5,6]. Growth rates as high as 17.5 metric tons per hectare per day have been reported by [6,7].

Propagation of water hyacinth occurs through both sexual reproduction via seeds and vegetative mechanisms, primarily through stolon formation and budding, with vegetative spread being the dominant route for rapid expansion [8]. Daughter ramets develop from stolons, and doubling times range from 6 to 18 days, depending on temperature and nutrient availability. The plant is characterized by dark, fibrous roots that can appear anchored when entangled in sediments, but it remains fundamentally free-floating [9]. Historical studies have shown that 10 individual plants were capable of producing 1610 plants vegetatively within 3 months [9].

Water hyacinth tolerates a typical range of physicochemical conditions. But it can survive in both acidic and alkaline waters, and optimal growth occurs in near-neutral conditions [5]. Growth is supported by temperatures ranging from 10–40 °C, with optimum development between 25–27.5 °C, though the species is sensitive to prolonged cold exposure [9]. Salinity is a major limiting factor for expansion in coastal environments [10] as salt concentrations in wastewater systems restrict its growth, with tolerance generally reported below 10 ppt (parts per thousand) salinity [6,8,11].

Despite its invasive nature, water hyacinth biomass has attracted growing interest for its beneficial applications. In rural and decentralized systems, it has been incorporated into wastewater treatment strategies, coupled with biogas generation and compost production [4]. Over recent decades, a variety of pathways have been developed, converting harvested biomass into energy products, bio-materials, and engineering applications [12]. Considering these research advancements, the development of structure management strategies that integrate ecological control with commercial utilization appears both necessary and promising.

Glycolipids, phenolic compounds, flavonoids, quinones, sterols, and other compounds have all been found in various parts of *Eichhornia crassipes* [13,14]. These compounds, along with the reported antimicrobial, antioxidant, anti-inflammatory, and antitumor properties of *E. crassipes*, suggest its potential as a valuable source of bioactive compounds for various value-added applications [15,16].

However, limited studies have combined GC-MS-based compound profiling with physicochemical characterization of different morphological parts of *E. crassipes*, including roots, stalks, leaves, and the whole plant. Therefore, this study aimed to characterize the chemical composition and physicochemical properties of different plant parts using GC-MS and other physicochemical and instrumental analyses to evaluate their different applications. This approach provides a better understanding of the chemical composition of *E. crassipes* and its potential for biomass valorization.

2. Materials & Methods

2.1. Sample Collection and Preparation for Analysis

Water hyacinth was collected during June–July 2025 from four distinct locations in and around Guwahati, India: (1) an industrial area at Amingaon, near the Indian Institute of Technology Guwahati (IITG) campus (26°12′09.9″ N, 91°41′14.3″E); (2) the Boragaon landfill area (26°06′57″N, 91°40′35.3″E); (3) a freshwater body near Deepor Beel (26°0′42.4″N, 91°4′29.0″E); and (4) a low-lying area close to an agricultural site (26°14′48.5″N, 91°45′56.1″E).

The selected plants were mature, with an average individual fresh weight ranging from approximately 85–100 g. At each site, around 30 independent plants were collected with sampling points spaced approximately 10 m apart. The plants selected for sampling were at a similar growth stage and comparable in size, with an approximate sampling depth of 15 cm. Before being analyzed, all of the materials that were collected were processed in the solid waste lab, IIT Guwahati. The plants were separated into root, shoot, stem and whole-plant samples. To increase the surface area for the samples, the maximum size of the water hyacinth particles was reduced to 1 cm. The average size was determined for each location sample after the water hyacinth parts were weighed individually. In order to analyze biological parameters, triplicate samples were gathered and kept at 4 °C. The samples were then dried and processed to obtain a homogeneous sample for the analysis. The prepared sample from each sampling location was analyzed in triplicate. These three measurements were technical replicates of the same composite sample and were not considered independent biological replicates. The results were presented as mean ± standard deviation of

the triplicate measurements. The same sample preparation and analytical procedures were followed for all sampling locations.

The moisture content was determined using Equation (1) after subsamples were dried for 24 h at 105 °C in a hot-air oven. Samples that had been dried were ground to fit through 0.2 mm sieves and kept for later analysis.

$$\text{Moisture Content (\%)} = (W1 - W2)/W1 \times 100 \quad (1)$$

Here, W1 is the initial weight of the sample, and W2 is the final weight of the sample after drying at 105 °C for 24 h.

2.2. Physicochemical and Nutritional Parameters

About 10 g of the sample and 100 mL of distilled water were combined in a 1:10 (w/v) ratio to measure pH and electrical conductivity. After that, the mixture was shaken horizontally for two hours at 120 rpm. The pH meter was then used to ascertain the suspension's pH. The EC meter was used to determine the suspension's conductivity. A crucible (W1) containing about 5 g of the sample was placed in a muffle furnace for 2 h at 550 °C in order to measure volatile solids. Following this period, the sample's final weight was noted as W2. The [17] standard method was used to calculate the sample's volatile solids:

$$VS = (5 - (W2 - W1))/5 \times 100 \quad (2)$$

Using the [17] standard method, total organic carbon was calculated by dividing the volatile solids value by a factor of 1.8 [18]. The total nitrogen (TN) content of the samples was determined using a Vario MACRO cube elemental analyzer (CHNS analyzer, Elementar Analysensysteme GmbH, Langenselbold, Germany). Spectrophotometric analysis was used to measure nitrate (NO_3^-) and ammoniacal nitrogen (NH_4^+) after extraction with a 2M KCl solution [19]. According to the [17], standard technique, the colorimetric method is used to determine total phosphorus and available phosphorus [18]. After the 0.2 g sample was digested in a block digester with 10 mL of mixed acid (H_2SO_4 and $HClO_4$ in a 5:1 ratio), the total concentration of Sodium (Na^+), potassium (K^+), Calcium (Ca^{2+}) was measured using a flame photometer (Systronics (India) Ltd., Ahmedabad, Gujarat, India) [18,19].

2.3. Heavy Metal Analysis

Atomic absorption spectroscopy (AAS) was used in triplicate for the heavy metal analysis. Total heavy metal concentrations were measured by digesting 0.2 g oven-dried sample (passed through a 212 µm sieve) with 10 mL of a H_2SO_4 and $HClO_4$ (5:1, v/v) acid mixture at 300 °C for 2 h. The concentration of the analyzed elements was quantified using appropriate calibration standards [20].

2.4. Biological Analysis

2.4.1. CO_2 Evolution Rate

A container was filled with 25 gm of fresh sample and about 10 g of oven-dried soda lime. According to [21], the CO_2 evolution was computed as follows:

$$CO_2 \text{ evolution (mg/gVS/day)} = (W2 - W1) \times 1000/W \times T \quad (3)$$

In Equation (3), W is the volatile solids weight of the sample (in grams), T is the duration of incubation (in hours), and W1 and W2 are the initial and final weights of the soda lime (in grams) following incubation at 25 °C and oven drying, respectively.

2.4.2. Soluble Biochemical Oxygen Demand (sBOD)

The material was placed on a horizontal shaker for 2 h after being diluted to a 1:10 ratio. After that, the solution was filtered, and the supernatant was collected for BOD_5 analysis.

$$sBOD = (S1 - S2)/P \quad (4)$$

Here, P stands for the volume of the sample diluted to a total volume of 300 mL using dilution water and S1 and S2 indicate the initial and final amounts of dissolved oxygen (DO) in the sample after 5 days of incubation, measured in mg/L.

2.4.3. Soluble Chemical Oxygen Demand (sCOD)

The sample was diluted 1:10 for sCOD analysis, and the filtrate was then subjected to the closed reflux procedure. This procedure involved mixing 2.5 mL of the filtered sample with 1.5 mL of $K_2Cr_2O_7$ and 3.5 mL of H_2SO_4 reagent in a COD vial. After 2 h of digestion at 150 °C, the mixture was cooled to room temperature. After that, it was titrated using a ferroin indicator against ferrous ammonium sulfate (FAS) until the color changed from green to deep red [18].

$$\text{sCOD} = (\text{A} - \text{B}) \times \text{M} \times 8000/\ \text{mL of sample} \quad (5)$$

In this case, M is the molarity of FAS, 8000 is the milliequivalent weight of oxygen multiplied by 1000 mL/L, and A and B are the volumes of FAS used for the blank and sample, respectively.

2.5. Instrumental Characterization

To investigate changes in functional groups across different locations, Fourier transform infrared spectroscopy (FTIR) was performed using a PerkinElmer FTIR spectrometer (Version 10.4.3). The FTIR spectrum was used to evaluate 1 mg of oven-dried sample that had been carefully combined with 100 mg of KBr powder. FTIR spectra were collected in the range of 450–4000 cm^{-1} using KBr powder as the background and a spectral resolution of 4 cm^{-1} with single scans per sample [22]. The SIGMA 300 FE-SEM (Carl Zeiss Microscopy GmbH, Jena, Germany) device was used to analyze *Eichhornia crassipes* biomass samples using field-emission scanning electron microscopy (FESEM) to detect sample deformations. The oven-dried sieved samples were mounted on aluminium stubs and gold-coated before analysis. FESEM images were acquired at an accelerating voltage (EHT) of 5 kV to examine the surface morphology of the samples. A monochromator-equipped Rigaku TTRAX III X-ray diffractometer (Tokyo, Japan) was used to record powder X-ray diffractograms (PXRD) to diffract a beam over 10–80° of a 2θ angle at a scanning rate of 2°/min on the oven-dried and sieved samples (212 µm) with a step size of 0.02° [23].

2.6. GC-MS Sample Preparation

Three 5 mL portions of diethyl ether were used to extract each 500 mg air-dried sample, while the sample was continuously agitated in a 25 mL retort. The non-soluble substance was then extracted using three sections of 10 mL of methanol and 5 mL n-hexane. At room temperature, each extraction cycle lasted 30 min. The solvent was extracted from the combined extracts using Whatman filter paper and a rotary evaporator set to 40 °C. 2 mL of methanol or diethyl ether was used to wipe away the residue that remained on the walls, and 0.5 mL of this solution was transferred into a 2 mL vial. 220 µL of pyridine and 80 µL of bis(trimethylsilyl)trifluoroacetamide (BSTFA) were added to the vial after the solvent had evaporated (these reagents were purchased from Sigma-Aldrich Co., St. Louis, MO, USA). To produce trimethylsilyl (TMS) derivatives, the reaction mixture was sealed and heated to 70 °C for 30 min [24].

2.7. GC-MS Analysis

An HP 6890 gas chromatograph with a mass selective detector (MSD 5973; Agilent Technologies, Santa Clara, CA, USA) was used to separate and evaluate TMS derivative solutions by GC-MS. This apparatus was equipped with a split injector, electronic pressure control, and an HP-5MS fused silica column (30 m × 0.25 mm, 0.25 µm film thickness). In continuous flow mode, the column's helium flow rate was 1 mL min^{-1}. The injector operated in split (1:20) mode at 250 °C. At 5 °C min^{-1}, the column temperature increased from 50 °C to 300 °C. The acquisition conditions for the MSD 5973 detector were as follows: the detector was maintained at 290 °C, and the transfer line temperature was equal to 250 °C. The ionization energy of 70 eV was used to get the EIMS spectra. From 35 to 600 a.m.u., detection was performed in full-scan mode.

3. Result and Discussion

3.1. Moisture Content, Volatile Solids, Total and Dissolved Organic Carbon

The highest moisture content (MC) was observed in plants collected from the agricultural run-off area, which may be related to the higher availability of nutrients and organic matter in the environment (see Figure 1a). However, moisture content can also vary depending on factors such as plant age, tissue composition, environmental conditions, and harvesting time [12,25]. The relatively lower MC observed in plants collected from the freshwater area may be associated with the differences in nutrient availability and surrounding environmental

conditions [25]. Thus, the variations in MC are likely influenced by a combination of factors rather than nutrient enrichment alone.

The organic matter in a sample is defined as Volatile Solids (VS), which vary across locations. The highest VS was observed in the industrial area in leaf and stem samples due to high organic matter deposition under polluted conditions, and in the Boragaon area for root and whole plant samples (see Figure 1b). On the other hand, the lowest VS was found in the freshwater body for leaf and whole-plant samples, and for root and stem in Boragaon and the industrial area, respectively, which indicates differences in metabolic adaptation capacity [25].

Total organic carbon (TOC) and dissolved organic carbon (DOC) showed noticeable spatial variation among the sampling sites. The industrial area recorded the highest TOC and DOC in leaf and stem tissues, likely due to elevated anthropogenic organic inputs and pollutant-associated carbon accumulation [26]. Total organic carbon (TOC) and dissolved organic carbon (DOC) were observed to be highest in the industrial area for leaf and stem, and also exhibited in agricultural area for root and whole plant due to carbon accumulation and nutrient runoff assimilation, respectively (see Figure 1c,d). In contrast, the lowest was found in the freshwater body, indicating low organic loading and nutrient availability.

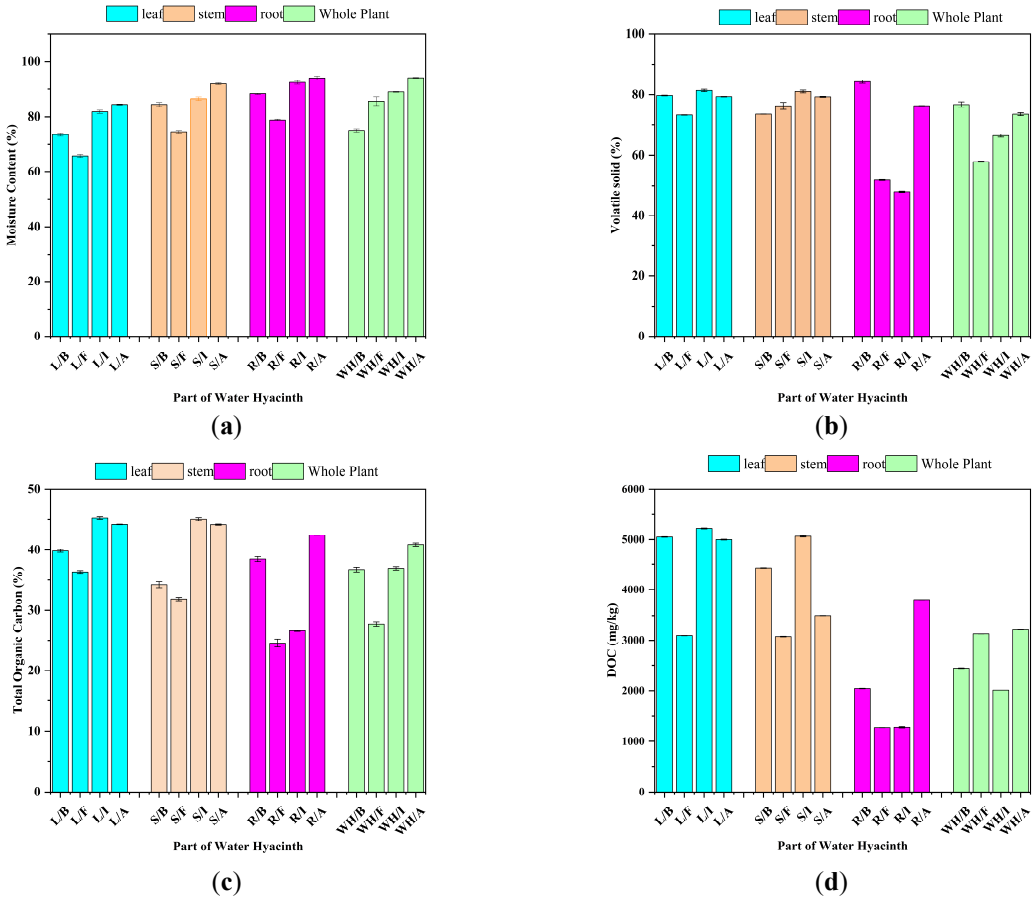

Figure 1. (**a**) Moisture content, (**b**) volatile solids, (**c**) TOC and (**d**) DOC of water hyacinth.

3.2. Nitrogen Dynamics

Nitrogen dynamics in water hyacinth reflect environmental nutrient accumulation and the plant's capacity for biomass adaptation. Total nitrogen (TN) and ammonium nitrogen (NH_{4+}) in the Boragaon area indicate nitrogen assimilation and active ammonification by microbial interactions in nutrient-enriched conditions (see Figure 2a,d) [2,27].

The highest nitrate (NO_3^-) was observed in the agricultural area, which indicates fertilizer deposition and promotes nitrogen uptake and biomass production capacity (see Figure 2b) [28]. In contrast, the industrial area exhibited lower TN and higher C/N ratios, suggesting nitrogen limitation relative to carbon accumulation, potentially due to pollutant stress affecting nutrient metabolism. Similarly, the lower nitrogen accumulation in the freshwater body indicates reduced external nutrient loading. Thus, these patterns enhance the capacity of water hyacinth to respond dynamically to site-specific nitrogen availability and its role as an efficient phytoremediator in nutrient-rich aquatic systems [25].

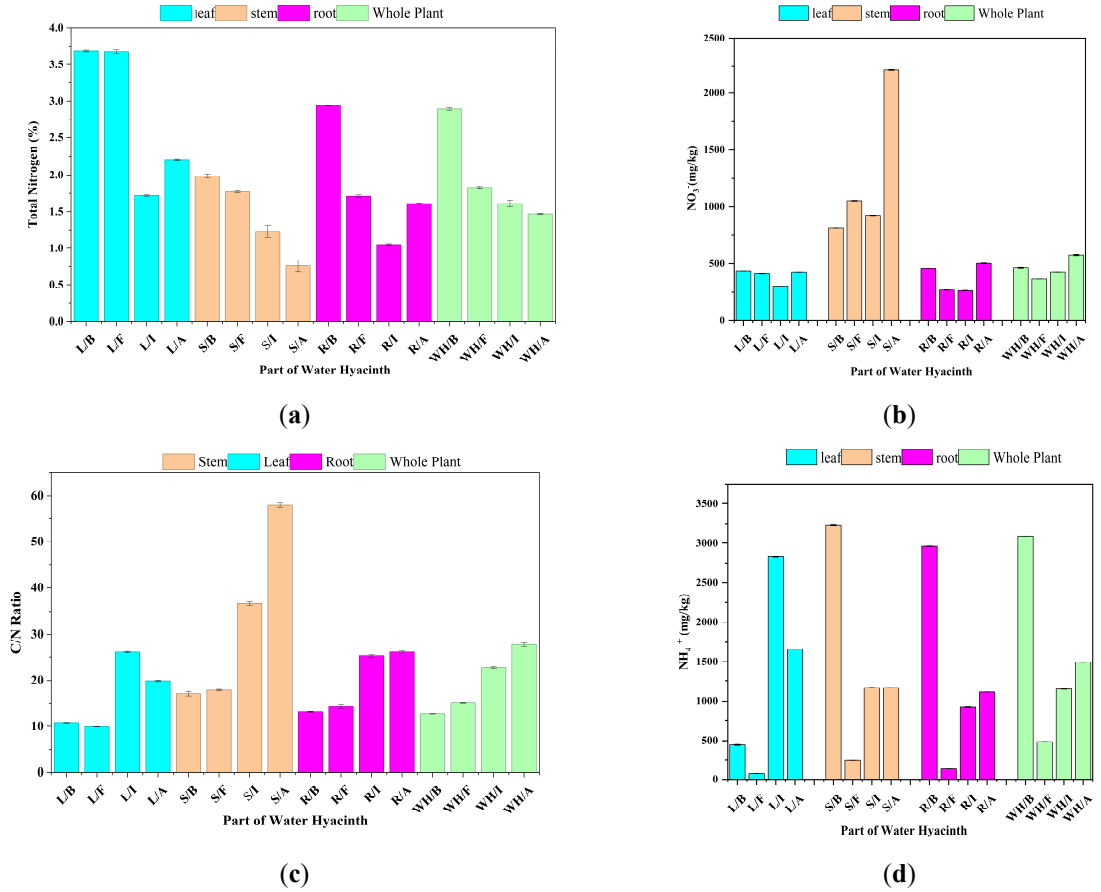

Figure 2. (**a**) TN, (**b**) NO_3^-, (**c**) C/N ratio and (**d**) NH_4^+ of water hyacinth.

3.3. Micro-Nutrients

The concentrations of Sodium (Na^+), Potassium (K^+), and Calcium (Ca^{2+}) varied among the sampling locations and plant tissues under different environmental conditions. Higher Na^+ concentrations were observed in leaf samples from Boragaon and stem, and root samples from the agricultural area, whereas lower Na^+ levels were found in the industrial area samples (see Figure 3a). Potassium concentrations were relatively higher in samples from the freshwater body, while lower values were observed in some tissues collected from the industrial area (see Figure 3b). Calcium showed the highest accumulation in roots from the freshwater body, whereas higher Ca^{2+} concentrations in aerial tissues were observed in samples from the agricultural area (see Figure 3c). These differences may be related to variations in nutrient availability, tissue composition, and the uptake and distribution of minerals within the plant [7]. However, the observed variations in Na^+, K^+, and Ca^{2+} concentrations indicate that both environmental conditions and plant tissue type may influence mineral accumulation in water hyacinth [6].

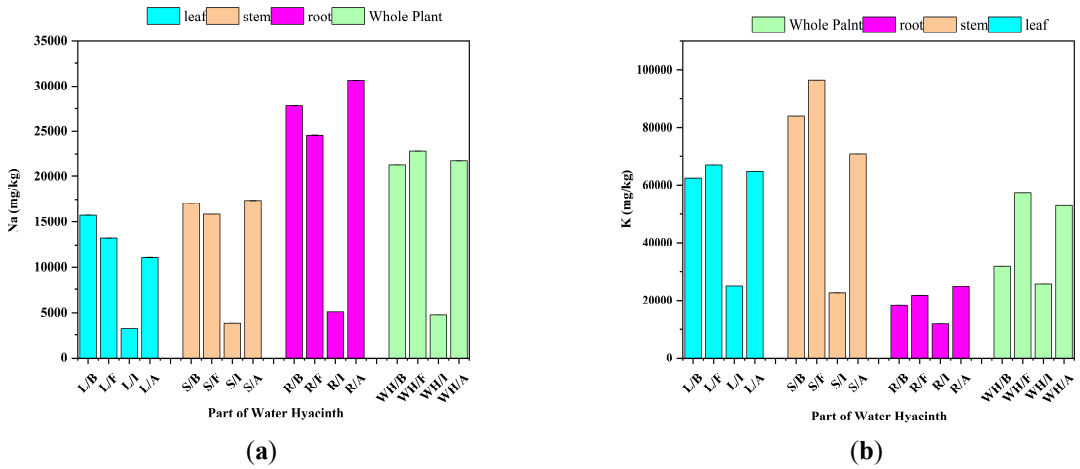

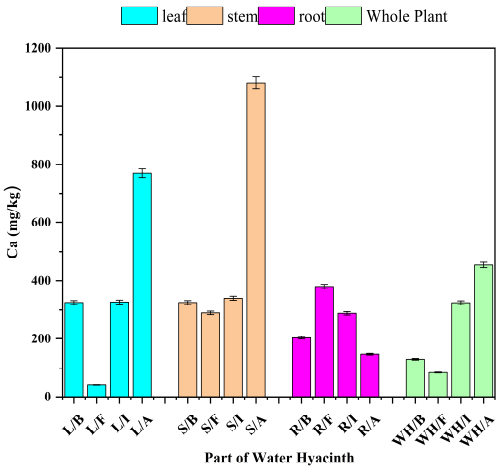

(**c**)

Figure 3. (**a**) Na^+, (**b**) K^+ and (**c**) Ca^{2+} of water hyacinth.

3.4. Biological Parameters

Soluble biochemical oxygen demand (sBOD) and chemical oxygen demand (sCOD) were observed to be the highest in the industrial area across all parts of the water hyacinth, indicating substantial accumulation of biodegradable and chemically oxidizable organic constituents due to anthropogenic discharge [29,30].

sBOD results indicate microbial oxygen consumption during decomposition processes, whereas high sCOD values suggest the presence of both organic and inorganic pollutants characteristic of industrial effluents (see Figure 4a,b). The freshwater body showed the lowest sCOD and sBOD among stem, root, and whole-plant samples (with leaf BOD being lowest in the agricultural area), indicating reduced organic loading and improved water quality.

The CO_2 evolution pattern varied among the plant tissues collected from different locations. The highest CO_2 evolution in leaf, stem, and whole plant samples from the freshwater body may be related to the presence of more easily degradable organic matter in these tissues (see Figure 4c). The higher CO_2 evolution observed in leaf samples from the freshwater body may be associated with differences in tissue composition and the availability of readily decomposable organic substrates [31]. The lower CO_2 evolution shown in the agricultural area may indicate lower availability of easily degradable substrates or greater stabilization of organic matter. However, the differences in CO_2 evolution suggest that the composition and environmental conditions experienced by the plants may influence the potential decomposition and carbon mineralization of their tissues during incubation [26].

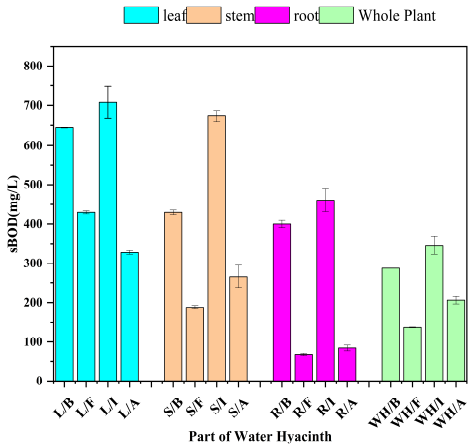

(**a**)

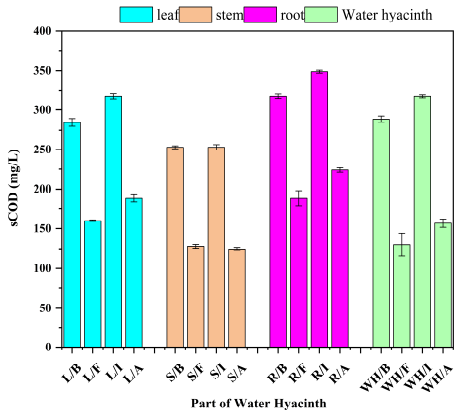

(**b**)

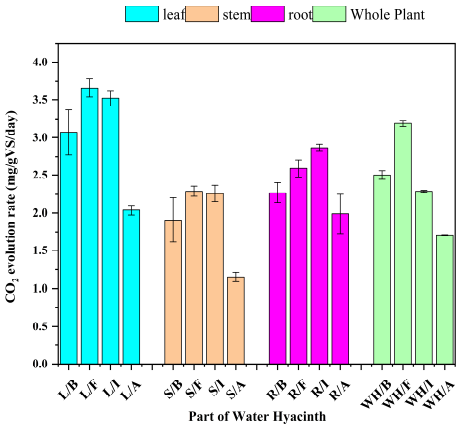

(**c**)

Figure 4. (**a**) sBOD, (**b**) sCOD and (**c**) CO_2 evolution rate of water hyacinth.

3.5. pH, EC, Total and Available Phosphorus

The pH and electrical conductivity (EC) of the aqueous extracts varied among plant tissues and sampling locations. The highest pH was recorded in leaf, stem, and root extracts from the freshwater body, while the lowest pH was observed in leaf and stem extracts from the Boragaon area and root and whole plant extracts from the industrial area (see Figure 5a). These differences may be related to variations in the chemical composition of the plant tissues and the soluble compounds released during extraction. Similarly, EC values differed among the sampling locations and plant parts. The highest EC was found in leaf and root extracts from the agricultural runoff area, whereas stem and whole plant extracts showed the highest EC in samples from the industrial area (see Figure 5b). The lowest EC was recorded in stem and whole plant extracts from the freshwater body, whereas leaf and root extracts showed the lowest values in the industrial area. These differences may be due to variations in the concentrations of soluble ions and water-soluble compounds present in the plant tissues [32].

Total phosphorus (TP) observed the highest concentrations in Boragaon for stem and root tissues, suggesting enhanced phosphorus loading and P mobilization in this area by sediment deposition (see Figure 5c). Phosphorus can be released from sediments through redox-mediated processes, increasing its availability for plant uptake [33]. In contrast, lower TP levels in leaf and whole plant samples from the freshwater body indicate lower anthropogenic input and limited phosphorus enrichment. Lower TP in agricultural and industrial sites for certain tissues may also indicate phosphorus immobilization through complexation with iron (Fe^{3+}), aluminum (Al^{3+}), or Calcium (Ca^{2+}), forming insoluble phosphate precipitates that restrict bioavailability [34].

Available phosphorus (AP) was the highest in Boragaon across all plant parts, which enhanced labile P availability driven by active organic matter mineralization and favorable redox conditions (see Figure 5d). Also, lower AP in the agricultural area suggests phosphorus fixation or rapid biological assimilation, reducing its exchangeable fraction. Industrial influences may further modify P speciation through pH and ionic shifts affected by sorption and desorption processes [35,36].

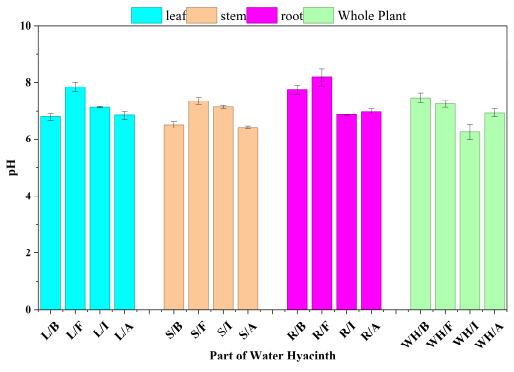

(**a**)

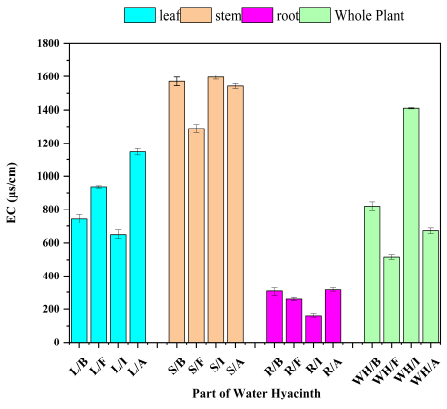

(**b**)

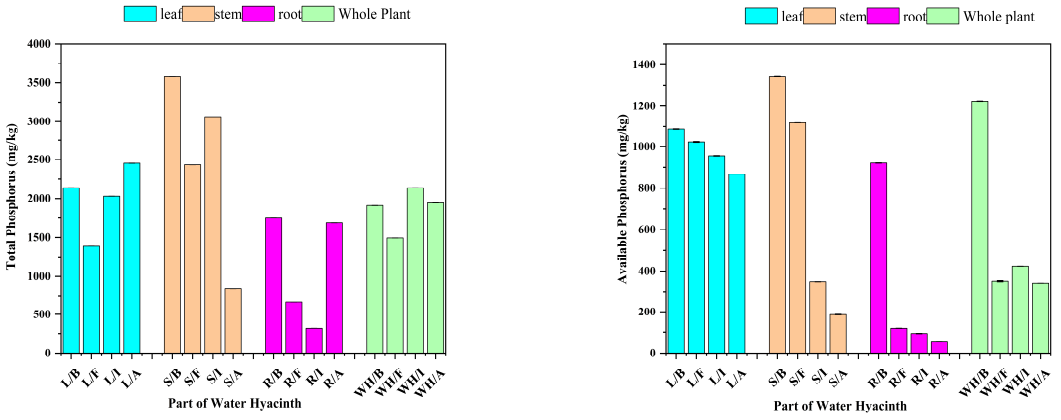

(**c**) (**d**)

Figure 5. (**a**) pH, (**b**) EC, (**c**) Total phosphorus and (**d**) Available phosphorus of water hyacinth.

3.6. Total Heavy Metals

The variation in total heavy metal content in water hyacinth showed significant spatial variability linked to contamination sources and environmental geochemistry. The industrial area exhibited the highest concentrations of Cd, Co, and Ni in most plant tissues, attributable to anthropogenic discharge and enhanced metal bioavailability. The agricultural area also showed the lowest Cd and Co levels, suggesting lower industrial metal input (see Figure 6a,b). Chromium (Cr) was highest in the freshwater body due to sediment remobilization under fluctuating redox conditions, on the other hand Boragaon Dumpsite showed the lowest Cr accumulation in leaf, root, and whole plant tissues, indicating possible immobilization or reduced bioavailable fractions (see Figure 6c). Copper (Cu) and Zinc (Zn) are essential micronutrients, which are found in the highest concentrations in the freshwater body because of physiological uptake under balanced environmental conditions (see Figure 6d,j). However, Cu accumulation in industrial leaf tissues suggests alterations in metal transport systems under stress conditions [4,37].

Iron (Fe) and manganese (Mn), both redox-sensitive elements, showed variable accumulation patterns influenced by site-specific oxygen availability and sediment chemistry (see Figure 6e,h). Fe in freshwater leaf and stem tissues may reflect greater solubility under favorable redox states, while variation in Mn across Boragaon and industrial areas indicates differential rhizospheric mobilization. Magnesium (Mg) is essential for chlorophyll structure and enzymatic activation, which was highest in the agricultural area, possibly due to fertilizer inputs, whereas reduced Mg in the industrial site may reflect ionic imbalance or competitive inhibition (see Figure 6g). Lead (Pb) accumulation was most significant in Boragaon (leaf and stem) and industrial root tissues, whereas freshwater samples consistently showed the lowest Pb levels, indicating limited contamination (see Figure 6i) [38].

Based on the mechanism, water hyacinth regulates heavy metal stress through selective uptake, chelation by phytochelatins and metallothioneins, sequestration into vacuoles, adsorption onto cell wall components, and restricted translocation to photosynthetically active tissues. These detoxification pathways help maintain ionic homeostasis and mitigate oxidative damage caused by reactive oxygen species under metal stress [39,40]. Therefore, the variations reflect an interplay between external contamination gradients, metal speciation and redox dynamics, and intrinsic physiological tolerance mechanisms, showing the strong phytoremediation capacity in heterogeneous aquatic ecosystems [41].

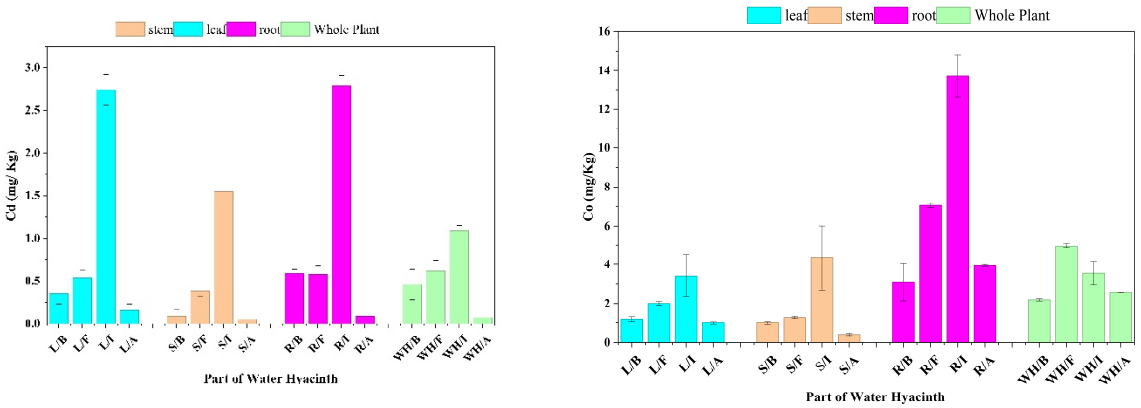

(**a**) (**b**)

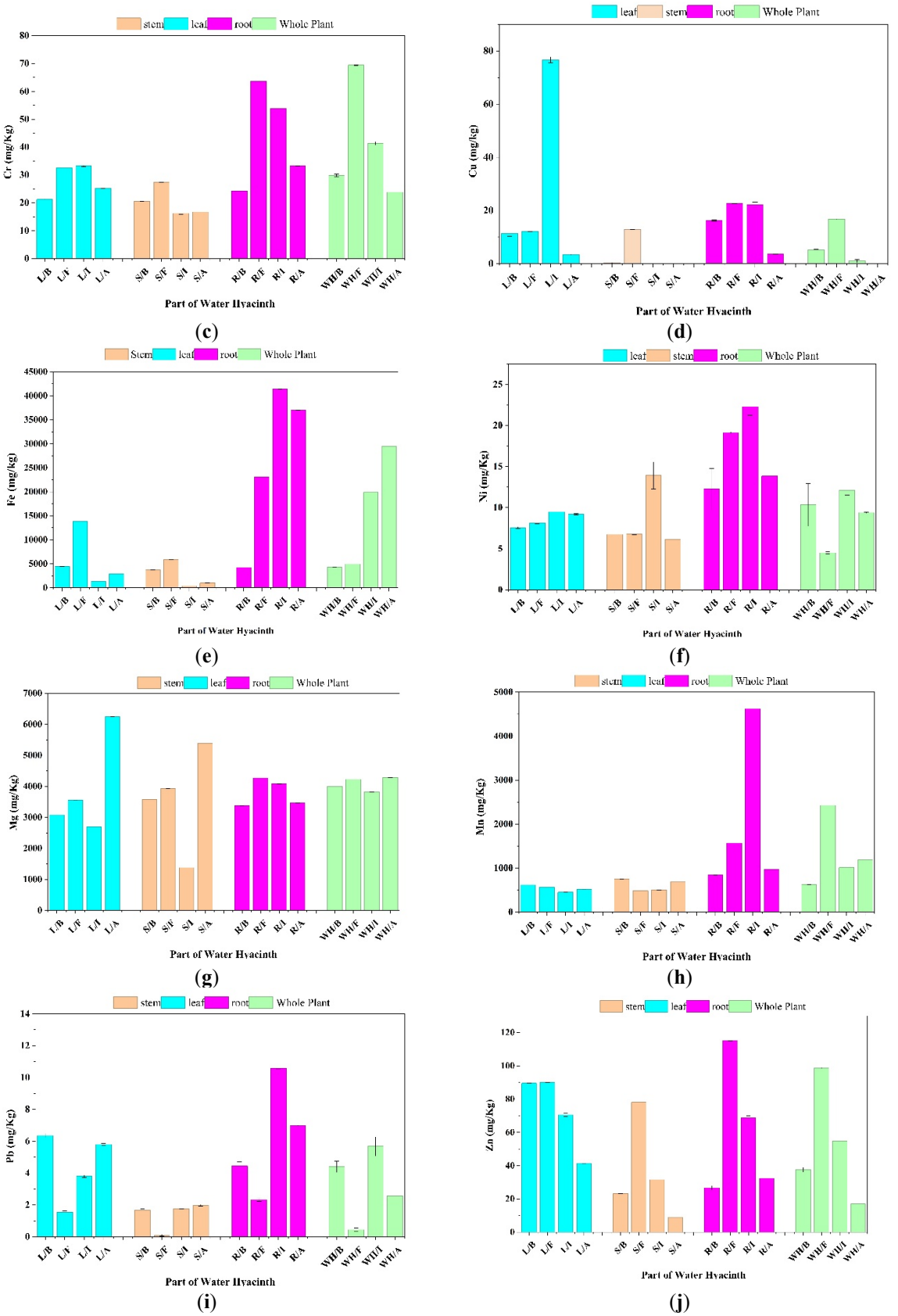

Figure 6. Concentrations of heavy metals in water hyacinth: (**a**) Cd, (**b**) Co, (**c**) Cr, (**d**) Cu, (**e**) Fe, (**f**) Ni, (**g**) Mg, (**h**) Mn, (**i**) Pb, and (**j**) Zn.

3.7. Instrumental Characterization

The FTIR spectra of *Eichhornia crassipes* biomass collected from the industrial site, Agricultural Run-off area, Boragaon Dump Site, and Freshwater body are provided in the Supplementary Material (Figure S1). The spectral variations were more significant among tissue types (leaf, stem, and root), indicating that biochemical

composition is primarily tissue-dependent [42,43]. A broad and intense band was observed in the 3650–3000 cm^{-1} region, corresponding to O-H stretching vibrations of hydroxyl groups associated with alcohols, phenols, and cellulose-bound water [44,45]. This band was comparatively stronger in the roots and whole-plant biomass, suggesting higher polysaccharide and lignocellulosic content. The peaks around 2920–2850 cm^{-1} were considered to be aliphatic C-H stretching, indicating lipid and structural carbohydrate components [23,44]. Leaf and stem tissues showed absorbance peaks in the 1750–1500 cm^{-1} region, which indicate the C=O stretching of carbonyl groups (carboxylic acids, esters, and amides) and aromatic skeletal vibrations. The 1495–1200 cm^{-1} region showed the C-O stretching and O-H bending vibrations, indicating the presence of hemicellulose, lignin, and other oxygenated functional groups [46]. These bands were clearly observed from the industrial and dump sites, suggesting structural modification and possible interaction with external contaminants. Roots consistently showed broader and more intense absorption bands across the 1200–800 cm^{-1} spectral range, corresponding to C-O-C and Si-O related vibrations. This region is linked with polysaccharide structures and potential mineral interactions [47,48]. The intensity of functional groups such as hydroxyl, carbonyl, and ether groups in roots supports their greater lignocellulosic complexity and higher density of adsorption capacity.

Field-emission scanning electron microscopy (FESEM) was used to examine the surface morphology of *Eichhornia crassipes* tissues collected from the four locations, see Supplementary Material (Figure S3). Microstructural differences were observed among tissues, indicating environmental influence on biomass architecture [42,49]. Leaf samples from the freshwater body generally retained intact epidermal surfaces with compact and continuous layers. Leaves from the Boragaon and industrial sites showed disturbed surface features characterized by irregular shapes, and the presence of adhered particulate matter. Agricultural runoff samples exhibited intermediate characteristics and slight surface unevenness. Stem tissues maintained a layered and fibrous organization in fresh water samples, and from contaminated sites showed structural distortion, flake detachment, and embedded surface agglomerates. Boragaon samples revealed denser particle accumulation within the matrix, suggesting enhanced interaction with external materials. Roots exhibited morphological alterations across all locations. Freshwater roots exhibited porous networks and defined cell wall contours, and Boragaon and industrial area samples showed partially encrusted surfaces with reduced visible porosity, indicating surface coverage by deposited materials. Agricultural run-off roots showed pore obstruction and surface scaling.

The X-ray diffraction (XRD) patterns of whole plant biomass and separated tissues (root, stem, and leaf) of *Eichhornia crassipes* are presented in Figure S2 (see Supplementary Material). All samples showed a combination of broad diffuse halos and distinct diffraction peaks within the 2θ range of 10–80°, indicating the coexistence of amorphous organic constituents and crystalline phases [43,50]. A broad feature between 20° and 25° was observed in all tissues, which is commonly associated with the semi-crystalline cellulose structure of cellulose-rich plant biomass. This feature appeared more pronounced in the root and whole plant samples; however, the XRD patterns alone do not permit a quantitative comparison of cellulose content among the tissues. A sharp reflection was detected near 26–28°, along with additional peaks around 39–41°, 50°, and 60–70°, indicating the presence of inorganic crystalline components integrated within the biomass matrix [51]. These reflections may be associated with the crystalline phases present in the biomass, including possible inorganic mineral components, although their specific mineralogical identity cannot be confirmed from the XRD patterns alone. The differences in peak intensity among the root, stem, leaf, and whole plant samples indicate variations in the relative contribution of crystalline and amorphous components. The whole plant sample showed a combined diffraction pattern reflecting the contributions of its different tissues and associated crystalline phases.

3.8. GC-MS Data Analysis

Various compounds have been identified by GC-MS using the described methodology. The most common identified compounds were acids, alcohols, hydrocarbons, aldehydes, esters and ethers in smaller percentages. Tables 1–4 represent the Boragaon dumpsite, agricultural runoff, freshwater bodies, and industrial areas biomass compound, respectively. In the industrial area, phenolic and highly carcinogenic compounds were found, whereas anti-inflammatory and antioxidant-like compounds were most common in the freshwater body.

Table 1. Boragaon dumpsite area.

Retention Time	Compound Name	Leaf	Stem	Root	Full Part	CAS Number
4.190	3-Bromo-N-butyl-4-methylbenzenesulfonamide	√				850429-68-4
4.190	N-Butyl 3-bromo 5-methylbenzenenesufonamide	√				1020252-93-0
4.290	Trifluoroacetoxypentadecane	√				1894-68-4
4.370	Trisiloxane, octamethyl	√	√	√	√	107-51-7
4.370	Eleutheroside B1	√	√	√	√	16845-16-2
4.254	2- Trifluroacetoxydodecane	√				1894-68-4
4.370	Canthin-6-one	√	√	√	√	479-43-6
4.370	Undecane	√	√	√	√	1120-21-4
7.652	Octane, 2,4,6-trimethyl	√	√		√	62016-37-9
9.784	Silane, cyclohexyldimethoxymethyl	√	√	√	√	1112-39-6
11.908	Heptane, 2,4,6-trimethyl	√	√	√	√	2613-61-8
11.707	Pentanoic acid, 1,1-dimethylpropyl ester	√				117421-32-6
15.960	Tridecane	√	√	√	√	629-50-5
14.918	Caryophyllene	√				87-44-5
15.608	Xanthosine	√				146-80-5
14.787	Nonadecane	√	√	√	√	629-92-5
16.395	Chlorpromazine	√				50-53-3
16.395	Phenol, 2,5-bis (1,1-dimethylethyl)-	√				5875-45-6
16.395	1-(9H-Carbazol-9-yl)-3-(1-piperidinyl)-2-propanol	√				91324-14-0
16.935	2,4-Di-tert-butylphenol	√	√			96-76-4
16.468	Butylated Hydroxytoluene	√	√	√		128-37-0
17.790	Caryophyllene oxide	√				1139-30-6
25.977	2-Hexyl-1-octanol	√	√		√	19780-79-1
21.965	Phytol	√	√		√	150-86-7
23.36	n-Hexadecanoic acid	√	√	√	√	57-10-3
25.233	Oxalic acid, allyl pentadecyl ester	√	√	√	√	-
21.897	Carbonic acid, eicosyl vinyl ester	√	√	√	√	-
9.795	Metazachlor		√	√	√	67129-08-2
16.399	Fraxidinglucoside		√	√	√	58970-71-1
25.977	Octadecanoic acid		√			57-11-4
30.137	Ipriflavone		√			35212-22-7
38.246	Aminopterin		√	√	√	54-62-6
38.246	Everzol Orange BN		√	√	√	1346500-15-9
38.303	Rhodomyrtone		√	√	√	468757-69-9
38.861	Phenol, 2,4-bis (1,1-dimethylethyl)-, phosphite (3:1)		√			31570-04-4
42.296	Silicic acid, diethyl bis(trimethylsilyl) ester		√		√	3555-45-1

Table 2. Agricultural run-off area.

Retention Time	Compound Name	Leaf	Stem	Root	Full Part	CAS Number
4.370	Trisiloxane, octamethyl	√	√	√	√	107-51-7
4.370	Eleutherside B1	√	√	√	√	16845-16-2
4.370	Canthin-6-one	√	√	√	√	479-43-6
4.370	Undecane	√	√	√	√	1120-21-4
7.652	Octane, 2,4,6-trimethyl	√	√	√	√	62016-37-9
10.644	Rutinose	√				90-74-4
9.799	Silane, cyclohexyldimethoxymethyl	√	√	√	√	1112-39-6
10.644	Heptane, 2,4,6-trimethyl	√	√	√	√	2613-61-8
15.960	Tridecane	√	√	√	√	629-50-5
15.460	Butylated Hydroxytoluene	√		√	√	128-37-0
18.460	(2,5-Dioxotetrahydrofuran-3-yl) acetic acid	√				4756-10-9
14.787	Nonadecane	√	√	√	√	629-92-5
21.685	Neophytadiene	√		√	√	504-96-1
23.304	3,5-Difluoro-4-iodoaniline		√			1542-34-3
16.413	Phenol, 2,6-bis (1,1-dimethylethyl)-4-methyl-, methylcarbama		√	√	√	1918-11-2
21.965	Phytol	√				150-86-7
23.316	n-Hexadecanoic acid	√	√	√	√	57-10-3
25.233	Oxalic acid, allyl pentadecyl ester	√	√	√	√	-
21.197	Carbonic acid, eicosyl vinyl ester	√	√			-
9.795	Metazachlor	√	√	√		67129-08-2
38.246	Aminopterin	√	√	√	√	54-62-6
38.246	Everzol Orange BN	√	√	√	√	1346500-15-9
38.303	Rhodomyrtone	√	√	√	√	468757-69-9
38.361	Phenol, 2,4-bis(1,1-dimethylethyl)-, phosphite (3:1)	√				31570-04-4
42.294	Desmethylverapamil	√	√	√	√	77326-93-3

Table 3. Freshwater body.

Retention Time	Compound Name	Leaf	Stem	Root	Full Part	CAS Number
4.370	Trisiloxane, octamethyl	√	√	√	√	107-51-7
4.370	Eleutherside B1	√	√	√	√	16845-16-2
4.370	Canthin-6-one	√	√	√	√	479-43-6
6.798	2,2-Dimethylpropionic acid, 4-methylpentyl ester	√		√		150588-62-8
4.370	Undecane	√	√	√	√	1120-21-4
7.652	Octane, 3,5-dimethyl-	√		√	√	15869-93-9
9.784	Silane, cyclohexyldimethoxymethyl	√	√	√	√	1112-39-6
10.538	Heptane, 2,4,6-trimethyl	√	√	√	√	2613-61-8
19.282	(2,5-Dioxotetrahydrofuran-3-yl) acetic acid	√				4756-10-9
7.782	Rutinose	√		√	√	90-74-4
11.806	Tridecane	√	√	√	√	629-50-5
12.27	Nonadecane	√				629-92-5
16.413	Phenol, 2,6-bis(1,1-dimethylethyl)-		√	√	√	1918-11-2
16.468	Butylated Hydroxytoluene	√	√	√	√	128-37-0
21.602	Oxirane, tetradecyl-	√	√			7320-37-8
21.965	Phytol	√				150-86-7
23.316	n-Hexadecanoic acid		√			57-10-3
25.233	Oxalic acid, allyl pentadecyl ester	√	√	√	√	-
22.837	Tetracosane	√	√	√	√	646-31-1
21.897	Carbonic acid, eicosyl vinyl ester			√		-
9.795	Metazachlor		√			67129-08-2
16.399	Fraxidinglucoside	√		√		58970-71-1
26.247	Valproic acid β-Dglucuronide	√				60113-83-9
38.265	Minocycline		√	√	√	10118-90-8
38.233	Aminopterin	√	√	√	√	54-62-6
28.246	Everzol Orange BN	√	√	√	√	1346500-15-9
38.303	Rhodomyrtone	√	√	√	√	468757-69-9
38.361	Phenol, 2,4-bis(1,1-dimethylethyl)-, phosphite (3:1)		√	√		31570-04-4
38.400	Desmethylverapamil	√	√			77326-93-3

Table 4. Industrial area.

Retention Time	Compound Name	Leaf	Stem	Root	Full Part	CAS Number
4.286	5-Nitro-2-furaldehyde semicarbazone	√				59-87-0
4.286	5-Hydroxymethyl-2-furancarboxylic acid	√				6338-41-6
4.286	3-Chloro-2-[(4-methylphenyl) sulfanyl]aniline	√				199803-23-1
4.370	Trisiloxane, octamethyl	√	√		√	107-51-7
4.370	Eleutherside B1	√	√		√	16845-16-2
4.774	L-Threitol		√			2319-57-5
5.556	Formamide, N,N-diethyl-	√	√			617-84-5
4.380	Canthin-6-one	√	√		√	479-43-6
7.663	Undecane	√	√	√	√	1120-21-4
13.010	Octane, 2,4,6-trimethyl	√	√	√	√	62016-37-9
7.780	2-Methoxy-N-(5-nitro-1,3-thiazol-2-yl) acetamide	√	√			64724-78-3
9.793	Silane, cyclohexyldimethoxymethyl	√	√	√	√	1112-39-6
10.641	Heptane, 2,4,6-trimethyl	√				2613-61-8
11.707	Pentanoic acid, 1,1-dimethylpropyl ester	√				117421-32-6
11.805	Tridecane	√	√	√	√	629-50-5
14.787	Nonadecane	√	√	√	√	629-92-5
16.395	Phenol, 2,5-bis (1,1-dimethylethyl)-	√				5875-45-6
23.304	Carmofur			√	√	61422-45-5
23.304	3,5-Difluoro-4-iodoaniline			√	√	1542-34-3
16.473	Butylated Hydroxytoluene	√	√	√	√	128-37-0
22.229	Phytol	√	√			150-86-7
23.299	Oxalic acid, allyl pentadecyl ester	√		√		-
22.837	Tetracosane	√				646-31-1
21.897	Carbonic acid, eicosyl vinyl ester	√	√	√	√	-
9.795	Metazachlor	√				67129-08-2
16.399	Fraxidinglucoside	√	√			58970-71-1
38.246	Aminopterin	√	√	√	√	54-62-6
38.246	Everzol Orange BN	√	√	√	√	1346500-15-9
38.303	Rhodomyrtone	√	√	√	√	468757-69-9
42.264	Silicic acid, diethyl bis(trimethylsilyl) ester	√				3555-45-1
6.969	2,2-Diethylacetamide		√	√		1114-38-1
38.316	Desmethylverapamil	√	√	√	√	77326-93-3

4. Application of Water Hyacinth

4.1. Bio-Energy Production

Water hyacinth has a promising bioenergy feedstock because it is fast-growing, widely available, non-edible, and naturally biodegradable. It has high cellulose and hemicellulose contents with low lignin (10%), making it more suitable for biological conversion than many terrestrial plants [52–54]. On the other side, other biomass often contains higher lignin (15–30%), which forms a rigid phenylpropanoid network around carbohydrates and limits microbial and enzymatic breakdown during fermentation [11,55].

However, a very high moisture content (over 90%), increases the cost and difficulty of harvesting and processing. But water hyacinth has been successfully explored for biogas production to meet rural household energy demands [56]. Pretreatment methods such as dilute sulfuric acid hydrolysis followed by saccharification and selected yeast fermentation can further enhance ethanol recovery [57]. Also, a mixture of 75% dry water hyacinth and 25% cow dung has been found to optimize methane yield, with one ton of dry biomass generating up to 370,000 L of biogas, indicating its potential as a sustainable alternative energy resource [11].

4.2. Compost Production

Water hyacinth can serve as a useful resource in farming, particularly as an organic fertilizer or mulch. With the growing interest in organic agriculture, especially in developed nations, this fast-growing plant offers a practical and low-cost nutrient source. Even after drying, it retains much of its nutrient value, and unlike many crop residues that may take 2–3 months to decompose, it can be composted in roughly 30 days [58,59].

When applied directly to fields as mulch or after composting, it has shown encouraging results. Crop yields of lady finger, potato, and tomato increased by 67%, 14%, and 90%, respectively, compared to fields without mulching [37,60]. Ref. [11] observed that when water hyacinth treated with high levels of glyphosate or 2,4-D was used as mulch, tomato growth declined compared to untreated plant material. Vermicomposting is also advantageous because once the plant passes through the earthworm gut, it loses its ability to reproduce vegetatively, making it safer and more manageable [61].

4.3. Wastewater Treatment

Water hyacinth has been widely studied at laboratory, pilot, and large operational scales for its ability to remove organic pollutants from wastewater systems [62]. It is widely recognized as an invasive species in many regions of the world, but it is a valuable biological resource in agriculture and waste management applications [63]. According to [64], plants cultivated in natural ponds and water channels are primarily utilized for water purification, and shorter harvesting intervals are recommended to enhance biomass productivity.

In dairy wastewater treatment studies, water hyacinth showed the remediation efficiency [33]. Over a 25-day treatment period, sequential monitoring of physicochemical parameters showed reductions in total solids (37%), calcium (5%), magnesium (47.5%), and total hardness (54%). The reductions were also observed in chloride, chromium, nitrous nitrogen, nitric nitrogen, pH, alkalinity, COD, BOD, and bicarbonates. This phytoremediation approach is considered suitable for industrial effluent management, as it can be applied to contaminated soils, groundwater, and wastewater using relatively low-cost and simple technological setups [65,66].

4.4. Biochar Production

Eichhornia crassipes produces a very high biomass yield and is rich in essential plant nutrients, making it a promising material for soil reclamation. However, the biomass is largely cellulosic. When applied directly to soil, this labile carbon fraction decomposes rapidly, leading to substantial carbon loss to the atmosphere. Transforming the biomass into biochar offers a more stable alternative, as it enhances carbon persistence and promotes long-term sequestration in soil [67,68].

Thermochemical processes, such as pyrolysis and gasification, are commonly employed to convert bulky and heterogeneous biomass into value-added products for various applications [69]. In pyrolysis, the original cellulosic carbon structures are thermally altered into more recalcitrant aromatic forms within biochar. This chemically stable carbon fraction decomposes slowly in soil, thereby increasing interest in biochar as a strategy to enhance soil carbon stocks. Thus, biochar is increasingly regarded as a promising tool for climate change mitigation [35].

4.5. Bioactive and Industrial Valorization Potential Based on GC-MS Metabolites

GC-MS profiling of *Eichhornia crassipes* reveals the presence of phenolic derivatives, fatty acids, sterols, long-chain hydrocarbons, and oxygenated organic compounds of industrial relevance. Phenolic constituents are widely recognized for antioxidant and anti-inflammatory properties due to their ability to neutralize reactive oxygen species and inhibit oxidative stress pathways [70]. The presence of phytosterols and lipid-derived metabolites also suggests potential therapeutic and nutraceutical applications, as plant sterols are linked with anti-inflammatory and cholesterol-modulating effects [13]. The fatty acids and long-chain hydrocarbons may serve as precursors for biodegradable lubricants, surfactants, and other green chemical formulations. Thus, the identified metabolites support the exploration of water hyacinth biomass as a source of natural antioxidants, bioactive compounds, and environmentally compatible industrial raw materials [71].

5. Conclusions

Physicochemical and instrumental assessments of *Eichhornia crassipes* revealed spatial and tissue-specific variability in biomass composition. The differences in Volatile solids, macronutrients, micronutrients, and heavy metals indicate environmental influences on carbon allocation and mineral assimilation. Root tissues showed relatively greater structural density and inorganic enrichment, whereas the surface part retained higher proportions of labile organic constituents.

Spectroscopic analysis confirmed heterogeneity in functional group distribution, particularly in polysaccharide-based bonds, aromatic structures, and oxygenated functional groups, reflecting differences in structural organization across sites. GC-MS metabolite analysis identified fatty acid derivatives, phenolic compounds, aliphatic hydrocarbons, and organic acids, with relative abundances varying with environmental conditions. This molecular variability indicates metabolic adaptation and biochemical plasticity within the biomass. A limitation of the present study is that the measurements were based on analytical replicates rather than independent biological replicates; further statistical analyses are needed to validate the observed differences. However, these findings of bulk physicochemical parameters and metabolomic signatures indicate that water hyacinth is compositionally dynamic rather than uniform. Such variability requires site-specific evaluation when considering downstream bio-based conversion processes.

Supplementary Materials

The additional data and information can be downloaded at: https://media.sciltp.com/articles/others/26091816 13559762/BCCN-26060277-SI.pdf. Figure S1: Fourier-transform infrared (FTIR) spectra of water hyacinth were collected from different locations at the Boragaon dump site, agricultural run-off, industrial area, and freshwater bodies. Figure S2: X-ray diffraction (XRD) patterns of water hyacinth were collected from different locations at the Boragaon dump site, agricultural runoff, industrial areas, and freshwater bodies. Figure S3: Field-emission scanning electron microscopy (FESEM) images of water hyacinth were collected from different locations at the Boragaon dump site, agricultural runoff, industrial areas, and freshwater bodies.

Author Contributions

S.A.: Conceptualization, data curation, formal analysis, investigation, methodology, resources, software, visualization, validation, writing—original draft, writing—review & editing. A.S.K.: Conceptualization, methodology, project administration, resources, supervision, validation, writing—review & editing. All authors have read and agreed to the published version of the manuscript.

Funding

This research received no external funding.

Institutional Review Board Statement

Not applicable.

Informed Consent Statement

Not applicable.

Data Availability Statement

The data generated and analyzed during the current study are available from the corresponding author upon reasonable request.

Acknowledgments

The authors are thankful to the School of Agro and Rural Technology, Centre for Environment, Department of Civil Engineering, and Central Instrument Facility (CIF), Indian Institute of Technology Guwahati, Assam, India, for providing space, instruments, and assistance in the smooth running of the research work.

Conflicts of Interest

The authors declare no conflict of interest.

Use of AI and AI-Assisted Technologies

During the preparation of this manuscript, the authors have used AI-assisted tools to support language refinement, paraphrasing, and improvement of readability.

References

1. Gupta, A.K.; Yadav, D. Biological control of water hyacinth. *Environ. Contam. Rev.* **2020**, *3*, 37–39. https://doi.org/10.26480/ecr.01.2020.37.39.
2. Vymazal, J. Removal of nutrients in various types of constructed wetlands. *Sci. Total Environ.* **2007**, *380*, 48–65. https://doi.org/10.1016/j.scitotenv.2006.09.014.
3. Lancar, L.; Krake, K. *Aquatic Weeds & Their Management*; International Commission on Irrigation and Drainage: New Delhi, India, 2002.
4. Singh, J.; Kalamdhad, A.S. Concentration and speciation of heavy metals during water hyacinth composting. *Bioresour. Technol.* **2012**, *124*, 169–179. https://doi.org/10.1016/j.biortech.2012.08.043.
5. Williams, A.E. Water hyacinth. In *Van Nostrand's Scientific Encyclopedia*; John Wiley & Sons: New York, NY, USA, 2006. https://doi.org/10.1002/0471743984.vse7463.pub2.
6. Gupta, B.; Huang, B. Mechanism of salinity tolerance in plants: Physiological, biochemical, and molecular characterization. *Int. J. Genom.* **2014**, *2014*, 701596. https://doi.org/10.1155/2014/701596.
7. Marschner, P. *Marschner's Mineral Nutrition of Higher Plants*, 3rd ed.; Academic Press: Amsterdam, Netherlands, 2011.
8. Wilson, J.R.; Holst, N.; Rees, M. Determinants and patterns of population growth in water hyacinth. *Aquat. Bot.* **2005**, *81*, 51–67. https://doi.org/10.1016/j.aquabot.2004.11.002.
9. Wilson, J.R.; Rees, M.; Holst, N.; et al. Water hyacinth population dynamics. In Proceedings of the Second Meeting of the Global Working Group for the Biological and Integrated Control of Water Hyacinth, Canberra, Australia, 9–12 October 2000; pp. 96–104.
10. Olivares, E.; Colonnello, G. Salinity gradient in the Manamo River, a dammed distributary of the Orinoco Delta, and its influence on the presence of Eichhornia crassipes and Paspalum repens. *Interciencia* **2000**, *25*. 242–248.
11. Rezania, S.; Ponraj, M.; Din, M.F.M.; et al. The diverse applications of water hyacinth with main focus on sustainable energy and production for new era: An overview. *Renew. Sustain. Energy Rev.* **2015**, *41*, 943–954. https://doi.org/10.1016/j.rser.2014.09.006.
12. Villamagna, A.M.; Murphy, B.R. Ecological and socio-economic impacts of invasive water hyacinth (*Eichhornia crassipes*): A review. *Freshw. Biol.* **2010**, *55*, 282–298. https://doi.org/10.1111/j.1365-2427.2009.02294.x.
13. Lakshminarayana, G.; Rao, K.S.; Pantulu, A.J.; et al. Composition of lipids in roots, stalks, leaves and flowers of *Eichhornia crassipes* (mart.) solms. *Aquat. Bot.* **1984**, *20*, 219–227. https://doi.org/10.1016/0304-3770(84)90088-3.
14. Vasu, K.; Goud, J.V.; Suryam, A.; et al. Biomolecular and phytochemical analyses of three aquatic angiosperms. *Afr. J. Microbiol. Res.* **2009**, *3*, 418–421. https://doi.org/10.5897/ajmr.9000134.
15. Aboul-Enein, A.M.; Al-Abd, A.M.; Shalaby, E.; et al. *Eichhornia crassipes* (mart) solms from water parasite to potential medicinal remedy. *Plant Signal. Behav.* **2011**, *6*, 834–836. https://doi.org/10.4161/psb.6.6.15166.
16. Shanab, S.M.M.; Shalaby, E.A. Biological activities and anticorrosion efficiency of water hyacinth (*Eichhornia crassipes*). *J. Med. Plants Res.* **2012**, *6*, 3950–3962. https://doi.org/10.5897/jmpr12.191.
17. Brandi, J.; Wilson-Wilde, L. Standard methods. In *Encyclopedia of Forensic Sciences*, 2nd ed.; Elsevier Inc.: London, UK; Waltham, MA, USA, 2013; pp. 522–527. https://doi.org/10.1016/b978-0-12-382165-2.00237-3.
18. Kauser, H.; Pal, S.; Haq, I.; et al. Evaluation of rotary drum composting for the management of invasive weed Mikania micrantha Kunth and its toxicity assessment. *Bioresour. Technol.* **2020**, *313*, 123678. https://doi.org/10.1016/j.biortech.2020.123678.

19. Saikia, S.; Maturi, K.C.; Prit, H.; et al. Application of municipal solid waste (MSW) char during rotary drum co-composting (RDC) of vegetable waste and its characterization. *Environ. Sci. Pollut. Res.* **2025**, *32*, 29917–29933. https://doi.org/10.1007/s11356-024-34332-4.
20. Maturi, K.C.; Haq, I.; Kalamdhad, A.S. Biodegradation of an intrusive weed *Parthenium hysterophorus* through in-vessel composting technique: Toxicity assessment and spectroscopic study. *Environ. Sci. Pollut. Res.* **2022**, *29*, 84600–84615. https://doi.org/10.1007/s11356-022-21816-4.
21. Kalamdhad, A.S.; Singh, Y.K.; Ali, M.; et al. Rotary drum composting of vegetable waste and tree leaves. *Bioresour. Technol.* **2009**, *100*, 6442–6450. https://doi.org/10.1016/j.biortech.2009.07.030.
22. Mandpe, A.; Yadav, N.; Paliya, S.; et al. Exploring the synergic effect of fly ash and garbage enzymes on biotransformation of organic wastes in in-vessel composting system. *Bioresour. Technol.* **2021**, *322*, 124557. https://doi.org/10.1016/j.biortech.2020.124557.
23. Paul, S.; Kauser, H.; Jain, M.S.; et al. Biogenic stabilization and heavy metal immobilization during vermicomposting of vegetable waste with biochar amendment. *J. Hazard. Mater.* **2020**, *390*, 121366. https://doi.org/10.1016/j.jhazmat.2019.121366.
24. Kotowska, U.; Piotrowska, A.; Isidorova, A.G.; et al. Gas chromatographic-mass spectrometric investigation of the chemical composition of the aquatic plant *Wolffia arrhiza* (Lemnaceae). *Oceanol. Hydrobiol. Stud.* **2013**, *42*, 181–187. https://doi.org/10.2478/s13545-013-0072-0.
25. Reddy, K.R.; Agami, M.; Tucker, J.C. Influence of nitrogen supply rates on growth and nutrient storage by water hyacinth (*Eichhornia crassipes*) plants. *Aquat. Bot.* **1989**, *36*, 33–43. https://doi.org/10.1016/0304-3770(89)90089-2.
26. Zhang, J.; Li, Y.; Liu, C.; et al. Concentration Levels, Biological Enrichment Capacities and Potential Health Risk Assessment of Trace Elements in *Eichhornia crassipes* from Honghu Lake, China. *Sci. Rep.* **2019**, *9*, 2431. https://doi.org/10.1038/s41598-018-36511-z.
27. Imaoka, T.; Teranishi, S. Rates of nutrient uptake and growth of the water hyacinth [*Eichhornia crassipes* (mart.) solms]. *Water Res.* **1988**, *22*, 943–951. https://doi.org/10.1016/0043-1354(88)90140-6.
28. Camargo, J.A.; Alonso, Á. Ecological and toxicological effects of inorganic nitrogen pollution in aquatic ecosystems: A global assessment. *Environ. Int.* **2006**, *32*, 831–849. https://doi.org/10.1016/j.envint.2006.05.002.
29. APHA; AWWA; WEF. *Standard Methods for the Examination of Water and Wastewater*, 21st ed.; Eaton, A.D., Clesceri, L.S., Rice, E.W.; et al., eds.; American Public Health Association: Washington, DC, USA, 2005.
30. Metcalf & Eddy; Tchobanoglous, G.; Burton, F.L.; et al. *Wastewater Engineering: Treatment and Reuse*, 4th ed.; McGraw-Hill: Boston, MA, USA, 2003.
31. Xie, J.; Gao, Y.; Xu, X.; et al. Effects of decomposition of submerged aquatic plants on CO_2 and CH_4 release in river sediment–water environment. *Water* **2023**, *15*, 2863. https://doi.org/10.3390/w15162863.
32. Gavrilaş, S.; Burescu, F.L.; Chereji, B.D.; et al. The impact of anthropogenic activities on the catchment's water quality parameters. *Water* **2025**, *17*, 1791. https://doi.org/10.3390/w17121791.
33. Barko, J.W.; Smart, R.M. Sediment-based nutrition of submersed macrophytes. *Aquat. Bot.* **1981**, *10*, 339–352. https://doi.org/10.1016/0304-3770(81)90032-2.
34. Gérard, F. Clay minerals, iron/aluminum oxides, and their contribution to phosphate sorption in soils—A myth revisited. *Geoderma* **2016**, *262*, 213–226. https://doi.org/10.1016/j.geoderma.2015.08.036.
35. Hinsinger, P. Bioavailability of soil inorganic P in the rhizosphere as affected by root-induced chemical changes: A review. *Plant Soil* **2001**, *237*, 173–195. https://doi.org/10.1023/a:1013351617532.
36. Penn, C.J.; Camberato, J.J. A critical review on soil chemical processes that control how soil pH affects phosphorus availability to plants. *Agriculture* **2019**, *9*, 120. https://doi.org/10.3390/agriculture9060120.
37. Lytle, C.M.; Lytle, F.W.; Yang, N.; et al. Reduction of Cr(VI) to Cr(III) by wetland plants: Potential for in situ heavy metal detoxification. *Environ. Sci. Technol.* **1998**, *32*, 3087–3093. https://doi.org/10.1021/es980089x.
38. Marchand, L.; Mench, M.; Jacob, D.L.; et al. Metal and metalloid removal in constructed wetlands, with emphasis on the importance of plants and standardized measurements: A review. *Environ. Pollut.* **2010**, *158*, 3447–3461. https://doi.org/10.1016/j.envpol.2010.08.018.
39. Clemens, S. Toxic metal accumulation, responses to exposure and mechanisms of tolerance in plants. *Biochimie* **2006**, *88*, 1707–1719. https://doi.org/10.1016/j.biochi.2006.07.003.
40. Sharma, S.S.; Dietz, K.J. The relationship between metal toxicity and cellular redox imbalance. *Trends Plant Sci.* **2009**, *14*, 43–50. https://doi.org/10.1016/j.tplants.2008.10.007.
41. Mishra, V.K.; Tripathi, B.D. Concurrent removal and accumulation of heavy metals by the three aquatic macrophytes. *Bioresour. Technol.* **2008**, *99*, 7091–7097. https://doi.org/10.1016/j.biortech.2008.01.002.
42. Bhattacharyya, P.; Bhaduri, D.; Adak, T.; et al. Characterization of rice straw from major cultivars for best alternative industrial uses to cutoff the menace of straw burning. *Ind. Crops Prod.* **2020**, *143*, 111919. https://doi.org/10.1016/j.indcrop.2019.111919.
43. Poletto, M.; Ornaghi Júnior, H.L.; Zattera, A.J. Native cellulose: Structure, characterization and thermal properties. *Materials* **2014**, *7*, 6105–6119. https://doi.org/10.3390/ma7096105.

44. Biyada, S.; Merzouki, M.; Elkarrach, K.; et al. Spectroscopic characterization of organic matter transformation during composting of textile solid waste using UV–visible spectroscopy, infrared spectroscopy and X-ray diffraction (XRD). *Microchem. J.* **2020**, *159*, 105314. https://doi.org/10.1016/j.microc.2020.105314.
45. Varma, V.S.; Nashine, S.; Sastri, C.V.; et al. Influence of carbide sludge on microbial diversity and degradation of lignocellulose during in-vessel composting of agricultural waste. *Ecol. Eng.* **2017**, *101*, 155–161. https://doi.org/10.1016/j.ecoleng.2017.01.022.
46. El Ouaqoudi, F.Z.; El Fels, L.; Lemée, L.; et al. Evaluation of lignocellulose compost stability and maturity using spectroscopic (FTIR) and thermal (TGA/TDA) analysis. *Ecol. Eng.* **2015**, *75*, 217–222. https://doi.org/10.1016/j.ecoleng.2014.12.004.
47. Qin, R.; Su, C.; Mo, T.; et al. Effect of excess sludge and food waste feeding ratio on the nutrient fractions, and bacterial and fungal community during aerobic co-composting. *Bioresour. Technol.* **2021**, *320*, 124339. https://doi.org/10.1016/j.biortech.2020.124339.
48. Zhang, J.; Zhang, T.; Ying, Y.; et al. Effects of different additives on the chemical composition and microbial diversity during composting of *Camellia oleifera* shell. *Bioresour. Technol.* **2021**, *330*, 124990. https://doi.org/10.1016/j.biortech.2021.124990.
49. Singh, N.; Balomajumder, C. Phytoremediation potential of water hyacinth (*Eichhornia crassipes*) for phenol and cyanide elimination from synthetic/simulated wastewater. *Appl. Water Sci.* **2021**, *11*, 144. https://doi.org/10.1007/s13201-021-01472-8.
50. French, A.D. Idealized powder diffraction patterns for cellulose polymorphs. *Cellulose* **2014**, *21*, 885–896. https://doi.org/10.1007/s10570-013-0030-4.
51. Ouma, V.O.; Agumba, D.O.; Weramwanja, P.M.; et al. Sustainable valorization of water hyacinth-derived lignocellulose towards functional applications. *Cleaner Water* **2025**, *4*, 100139. https://doi.org/10.1016/j.clwat.2025.100139.
52. Bolenz, S.; Omran, H.; Gierschner, K. Treatments of water hyacinth tissue to obtain useful products. *Biol. Wastes* **1990**, *33*, 263–274. https://doi.org/10.1016/0269-7483(90)90130-k.
53. Gressel, J. Transgenics are imperative for biofuel crops. *Plant Sci.* **2008**, *174*, 246–263. https://doi.org/10.1016/j.plantsci.2007.11.009.
54. Gutiérrez, E.; Huerto, R.; Saldaña, P.; et al. Strategies for waterhyacinth (*Eichhornia crassipes*) control in Mexico. *Hydrobiologia* **1996**, *340*, 181–185. https://doi.org/10.1007/bf00012752.
55. Varma, V.S.; Dhamodharan, K.; Kalamdhad, A.S. Characterization of bacterial community structure during in-vessel composting of agricultural waste by 16S rRNA sequencing. *3 Biotech* **2018**, *8*, 301. https://doi.org/10.1007/s13205-018-1319-7.
56. Chuang, Y.S.; Lay, C.H.; Sen, B.; et al. Biohydrogen and biomethane from water hyacinth (*Eichhornia crassipes*) fermentation: Effects of substrate concentration and incubation temperature. *Int. J. Hydrogen Energy* **2011**, *36*, 14195–14203. https://doi.org/10.1016/j.ijhydene.2011.04.188.
57. Poddar, K.; Mandal, L.H.; Banerjee, G.C. Studies on water hyacinth *Eichhornia crassipes* chemical composition of the plant and water from different habitats. *Indian Vet. J.* **1991**, *68*, 833–837.
58. Sannigrahi, A.K.; Chakrabortty, S.; Borah, B.C. Large scale utilization of water hyacinth (*Eichhornia crassipes*) as raw material for Vermi composting and surface mulching in vegetable cultivation. *Ecol. Environ. Conserv.* **2002**, *8*, 269–271.
59. Stocker, R.K.; Haller, W.T. Residual effects of herbicide-treated *Eichhornia crassipes* used as a soil amendment. *Hydrobiologia* **1999**, *415*, 329–333. https://doi.org/10.1023/a:1003877432409.
60. Akçin, G.; Saltabas, Ö.; Afsar, H. Removal of lead by water hyacinth (*Eichhornia crassipes*). *J. Environ. Sci. Health Part A Environ. Sci. Eng. Toxicol.* **1994**, *29*, 2177–2183. https://doi.org/10.1080/10934529409376172.
61. Woomer, P.L.; Muzira, R.; Bwamiki, D.; et al. Biological management of water hyacinth waste in Uganda. *Biol. Agric. Hortic.* **2000**, *17*, 181–196. https://doi.org/10.1080/01448765.2000.9754841.
62. da Costa, R.H.R.; Bavaresco, A.S.L.; Medri, W.; et al. Tertiary treatment of piggery wastes in water hyacinth ponds. *Water Sci. Technol.* **2000**, *42*, 211–214. https://doi.org/10.2166/wst.2000.0645.
63. de Casabianca, M.L.; Laugier, T.; Posada, F. Petroliferous wastewaters treatment with water hyacinths (raffinerie de provence, France): Experimental statement. *Waste Manag.* **1995**, *15*, 651–655. https://doi.org/10.1016/0956-053x(96)00012-8.
64. Lu, J.; Fu, Z.; Yin, Z. Performance of a water hyacinth (*Eichhornia crassipes*) system in the treatment of wastewater from a duck farm and the effects of using water hyacinth as duck feed. *J. Environ. Sci.* **2008**, *20*, 513–519. https://doi.org/10.1016/s1001-0742(08)62088-4.
65. Sooknah, R.D.; Wilkie, A.C. Nutrient removal by floating aquatic macrophytes cultured in anaerobically digested flushed dairy manure wastewater. *Ecol. Eng.* **2004**, *22*, 27–42. https://doi.org/10.1016/j.ecoleng.2004.01.004.
66. Sushilkumar. Aquatic weeds problems and management in India. *Indian J. Weed Sci.* **2011**, *43*, 118–138.
67. Jeffery, S.; Verheijen, F.G.A.; van der Velde, M.; et al. A quantitative review of the effects of biochar application to soils on crop productivity using meta-analysis. *Agric. Ecosyst. Environ.* **2011**, *144*, 175–187. https://doi.org/10.1016/j.agee.2011.08.015.
68. Masto, R.E.; Kumar, S.; Rout, T.K.; et al. Biochar from water hyacinth (*Eichhornia crassipes*) and its impact on soil biological activity. *Catena* **2013**, *111*, 64–71. https://doi.org/10.1016/j.catena.2013.06.025.

69. Kim, K.H.; Kim, J.Y.; Cho, T.S.; et al. Influence of pyrolysis temperature on physicochemical properties of biochar obtained from the fast pyrolysis of pitch pine (*Pinus rigida*). *Bioresour. Technol.* **2012**, *118*, 158–162. https://doi.org/10.1016/j.biortech.2012.04.094.
70. Rice-Evans, C.; Miller, N.; Paganga, G. Antioxidant properties of phenolic compounds. *Trends Plant Sci.* **1997**, *2*, 152–159. https://doi.org/10.1016/s1360-1385(97)01018-2.
71. Silva, R.P.; de Melo, M.M.R.; Silvestre, A.J.D.; et al. Polar and lipophilic extracts characterization of roots, stalks, leaves and flowers of water hyacinth (*Eichhornia crassipes*), and insights for its future valorization. *Ind. Crops Prod.* **2015**, *76*, 1033–1038. https://doi.org/10.1016/j.indcrop.2015.07.055.